

Light curves of tidal disruption events in active galactic nuclei

Chi-Ho Chan^{1,2}, Tsvi Piran¹, and Julian H. Krolik³

¹Racah Institute of Physics, Hebrew University of Jerusalem, Jerusalem 91904, Israel

²School of Physics and Astronomy, Tel Aviv University, Tel Aviv 69978, Israel

³Department of Physics and Astronomy, Johns Hopkins University, Baltimore, MD 21218, USA

October 30, 2020

ABSTRACT

The black hole of an active galactic nucleus is encircled by an accretion disk. The surface density of the disk is always too low to affect the tidal disruption of a star, but it can be high enough that a vigorous interaction results when the debris stream returns to pericenter and punches through the disk. Shocks excited in the disk dissipate the kinetic energy of the disk interior to the impact point and expedite inflow toward the black hole. Radiatively efficient disks with luminosity $\gtrsim 10^{-3}$ Eddington have a high enough surface density that the initial stream–disk interaction leads to energy dissipation at a super-Eddington rate. Because of the rapid inflow, only part of this dissipated energy emerges as radiation, while the rest is advected into the black hole. Dissipation, inflow, and cooling balance to keep the bolometric luminosity at an Eddington-level plateau whose duration is tens of days, with an almost linear dependence on stellar mass. After the plateau, the luminosity decreases in proportion to the disk surface density, with a power-law index between -3 and -2 at earlier times, and possibly a steeper index at later times.

Key words: galaxies: nuclei – accretion, accretion disks – black hole physics – hydrodynamics

1. INTRODUCTION

When a star of mass M_\star and radius r_\star approaches a black hole of mass M_h on an orbit whose pericenter r_p is comparable to or smaller than the tidal radius $r_t \equiv r_\star (M_\star/M_h)^{-1/3}$ (Hills 1975), the tidal gravity of the black hole rips the star asunder (e.g., Rees 1988), leading to a tidal disruption event (TDE). The disruption takes place very close to the black hole: in units of the gravitational radius $r_g \equiv GM_h/c^2$, the tidal radius is

$$r_t \approx 50 r_g \left(\frac{M_h}{10^6 M_\odot} \right)^{-2/3} \left(\frac{M_\star}{M_\odot} \right)^{-1/3} \left(\frac{r_\star}{r_\odot} \right). \quad (1)$$

The mass return time, determined by the specific energy of the most bound debris, is the timescale on which this part of the debris returns to pericenter:

$$t_{\text{mb}} \sim 40 \text{ d} \times \left(\frac{M_h}{10^6 M_\odot} \right)^{1/2} \left(\frac{M_\star}{M_\odot} \right)^{-1} \left(\frac{r_\star}{r_\odot} \right)^{3/2} \left(\frac{r_p}{r_t} \right)^3. \quad (2)$$

General relativistic simulations of TDEs starting from stars with realistic structures reveal that these quantities are accurate only within a factor of ~ 2 (Ryu et al. 2020).

The black hole of an active galactic nucleus (AGN) is girdled by an accretion disk. When a TDE happens in the vicinity of such a black hole, the passage of the star through the disk leaves the disk largely intact, and the disruption proceeds as if the disk were absent. However, upon return to the vicinity of the black hole, the debris of the disrupted star, being much more extended and dilute than the star, can interact with the disk in a more interesting way (Kochanek 1994; see also Kathirgamaraju et al. 2017).

As we shall argue later, the stream typically has much more inertia than the disk, so it acts as an immovable obstacle to disk rotation. Shocks form where the disk runs into the stream, and

the shocks dissipate disk kinetic energy. When the disk surface density is large enough, the dissipation rate can be highly super-Eddington. This sort of shock dissipation could serve as the energy source for a bright flare different from the energy sources in ordinary TDEs, namely, accretion of any rapidly circularized debris (e.g., Rees 1988) and shocks due to stream self-interaction (Piran et al. 2015).

In Chan et al. (2019), we performed the first hydrodynamics simulations of the collision between the debris stream of a TDE and the pre-existing accretion disk of an AGN. We found that, as long as the stream is much heavier than the disk, our simulation results are sensitive only to how dense the disk is, not how dense the stream is. This observation allows us to extrapolate our simulation results to even heavier streams and make quantitative predictions, even though our simulations did not explicitly cover that regime.

We begin by highlighting the most salient simulation results in §2. Based on these results, we estimate in §3 the bolometric light curve expected when a debris stream tears through the disk. In §4, we scrutinize the dependence of the light curve on black hole mass and disk properties, and we present sample light curves. This discussion is followed by a comparison with previous theoretical models and observations in §5. We end with our conclusions in §6.

2. SUMMARY OF SIMULATIONS

In Chan et al. (2019), we simulated the collision between the debris stream of a TDE and the pre-existing accretion disk of an AGN. As illustrated in Figure 1, a parabolic stream, representing the returning debris, strikes the disk perpendicularly from above as it reaches pericenter. To study late-time behavior, here we extend the simulations from the original duration of ~ 12 d to double that. The longer duration is still a fraction of t_{mb} , so it is

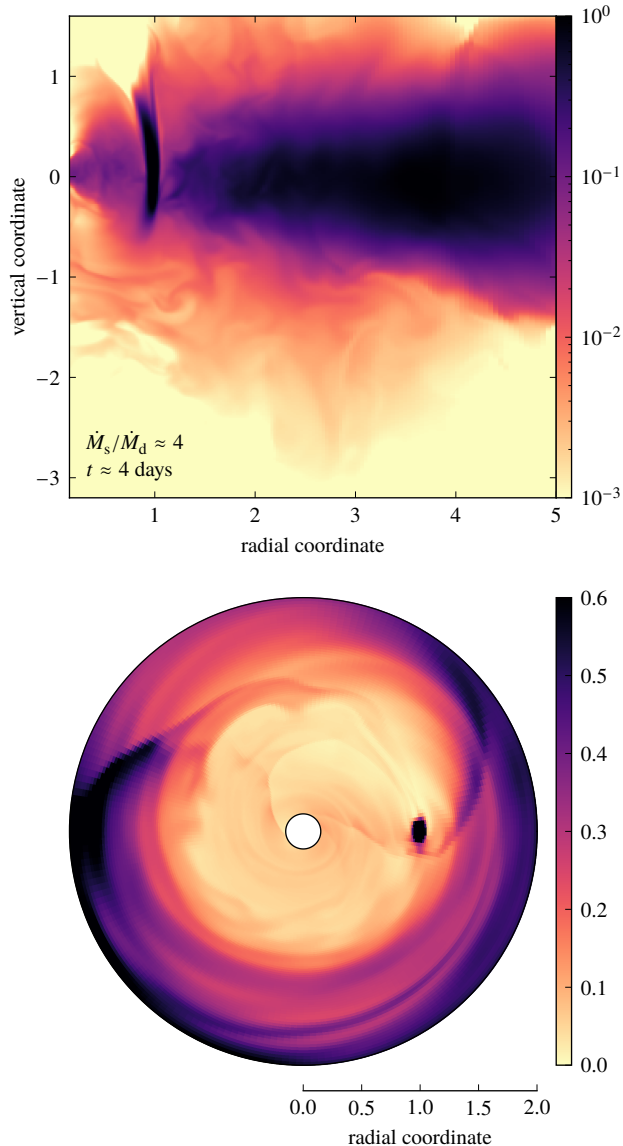


Figure 1. Density snapshot of one simulation in Chan et al. (2019). The top panel is a poloidal slice through the stream impact point with colors in logarithmic scale. The pericenter part of the stream, visible as a vertical structure, penetrates the disk with little difficulty, and energy dissipation makes the disk around the stream geometrically thick. The bottom panel is a midplane slice with colors in linear scale. The dark dot is a section of the stream, and spiral shocks are discernible interior to the stream. The density unit is arbitrary.

reasonable to keep the stream conditions constant.

We adopt as fiducial parameters $M_\star = M_\odot$, $r_\star = r_\odot$, and $r_p = r_t$. Since our interest is in disk physics, the relevant timescale is the disk orbital time at the impact point, which is by definition 2π times the stellar dynamical time:

$$t_{\text{orb}} = 2\pi \left(\frac{r_p^3}{GM_h} \right)^{1/2} = 2\pi \left(\frac{r_\star^3}{GM_\star} \right)^{1/2} \approx 3 \text{ h}. \quad (3)$$

The independence of t_{orb} on M_h means that our results, quoted in units of days, are valid for all M_h .

The most important parameter governing the collision is \dot{M}_s/\dot{M}_d , the ratio of the mass current of the stream to the mass

current of the disk rotating under the stream footprint. We shall see in §4 that $\dot{M}_s/\dot{M}_d \gtrsim 1$ typically; in other words, the stream has too much inertia to be affected by the disk, and it obstructs the rotating disk instead.

The collision excites multiple spiral shocks in the disk inside the stream impact radius. The shocks remove angular momentum and dissipate kinetic energy, thereby clearing out the inner disk within several t_{orb} . Magnetohydrodynamic (MHD) stresses are ignored in the simulations, but they act much more slowly than shocks. The top-left panel of Figure 2 tells us that the inflow time t_{infl} , or the time it takes shocks to redirect gas toward the black hole, gradually declines over the course of the event, from ~ 1 d at the start to ~ 0.4 d at $\gtrsim 10$ d.

As impact with the disk shaves off part of the stream, the inner disk mass is partially replenished with stream material. The inner disk mass is determined by the balance between inflow and replenishment. The longer simulations make clear this dynamic. The top-center panel of Figure 2 demonstrates that the inner disk mass drops roughly in proportion to the disk surface density Σ at the impact point. The top-right panel shows that $\gamma \equiv d \ln \Sigma / d \ln t$ lies between -3 and -2 toward the end of the simulations, and the decrease of Σ gradually steepens over time. We emphasize that the time-evolution of Σ is due to mechanisms wholly unrelated to those determining the power-law decay of the mass return rate at $t \gtrsim t_{\text{mb}}$.

The dissipated energy heats up the inner disk. As portrayed in the bottom-left panel of Figure 2, heating raises the disk aspect ratio at the impact point to $H/r_p \sim \frac{1}{2}$. The cooling time t_{cool} is the time the inner disk takes to release its internal energy as radiation, including the time needed to convert internal energy to radiation, and the time needed for radiation to escape through free streaming, diffusion, or vertical advection due to convection and magnetic buoyancy. Because electron scattering dominates the opacity in these circumstances, the diffusion time is $\sim \tau H/c$, where $\tau = \Sigma \kappa_T$ is the Thomson optical depth and κ_T is the cross section per mass for Thomson scattering. The diffusion time is long because τ drops rather slowly while $H/r_p \lesssim 1$ is much larger than in the unperturbed disk; in fact, the diffusion time is typically $\gtrsim t_{\text{infl}}$ at early times. The cooling time could be even longer because it also takes into account the radiation time. This means most of the radiation is trapped in the inflow toward the black hole and only a small fraction escapes.

3. ESTIMATION OF BOLOMETRIC LUMINOSITY

The swift inflow in the perturbed inner disk could produce a flare. Similar to a steady-state disk, the energy of the flare ultimately comes from the release of the gravitational energy of the disk gas. The contrast with a steady-state disk is twofold: first, dissipation and inflow happen on much shorter timescales; second, mass resupply from the stream allows more energy to be released than the gravitational energy possessed by the unperturbed disk.

We proposed in Chan et al. (2019) a crude estimate for the bolometric luminosity $L_c(t)$ of the collision-induced flare. Here we use the modified form

$$L_c \sim Q \min(1, t_{\text{infl}}/t_{\text{cool}}), \quad (4)$$

where $Q(t)$ is the energy dissipation rate. This equation encapsulates a competition between the inner disk releasing its internal energy as radiation, represented by t_{cool} , and the inflow

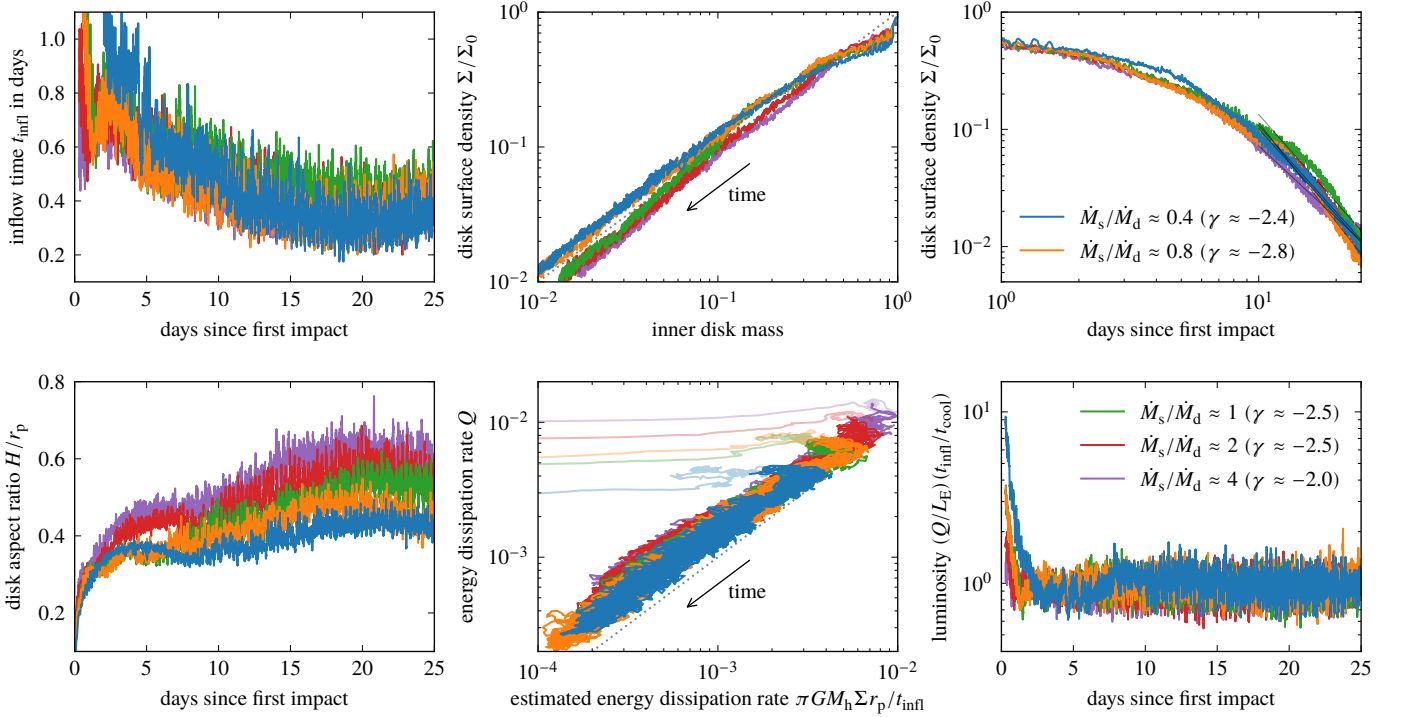


Figure 2. Diagnostics of the simulations in Chan et al. (2019), doubled in duration to study late-time behavior. The legend in the right column applies to all panels. The top-left panel shows the inflow time, that is, the inner disk mass divided by the inflow rate onto the black hole. The top-center panel shows the correlation between the inner disk mass and the disk surface density Σ at the impact point, measured from the midplane to infinity; both quantities are normalized to their initial values, and the dotted line marks a one-to-one ratio. The top-right panel shows Σ as a fraction of its initial value; the thin lines are power-law fits to late-time behavior and γ in the legend is the power-law index. The bottom-left panel shows the disk aspect ratio at the impact point. The bottom-center panel compares the energy dissipation rate estimated with Equation (6) and that measured directly from the simulations, both in arbitrary units; early-time data are plotted in a lighter color to highlight the late-time trend, and the dotted line marks a one-to-one ratio. The bottom-right panel shows the estimate of bolometric luminosity as defined in Chan et al. (2019), divided by the Eddington luminosity. The more accurate Equation (4) reduces to this estimate in the limit $t_{\text{infl}}/t_{\text{cool}} \lesssim 1$, which likely holds at early times when Σ is still relatively large.

sweeping this radiation into the black hole, represented by t_{infl} . When $t_{\text{infl}}/t_{\text{cool}} \lesssim 1$, the ratio $t_{\text{infl}}/t_{\text{cool}}$ estimates the fraction of dissipated energy the inner disk manages to radiate away; when $t_{\text{infl}}/t_{\text{cool}} \gtrsim 1$, all the dissipated energy is radiated away before the gas is accreted, so $L_c \sim Q$. Equation (4) is only an estimate; the true luminosity must be determined by performing time-dependent radiative transfer on the actual distribution of heating and opacity.

The top-left panel of Figure 2 and Equation (3) together tell us that

$$t_{\text{infl}} \sim 4t_{\text{orb}}. \quad (5)$$

Gas does not plunge into the black hole; rather, it spirals inward along trajectories that shift from quasi-circular near the impact radius to more eccentric at smaller radii. When disk material strikes the obstacle posed by the stream, it loses a large part of both its angular momentum and its energy; when it is deflected by shocks at smaller radii, the fractional loss of angular momentum is greater. For this reason, the heating rate as a function of time is reasonably estimated by the orbital kinetic energy of gas orbiting at the impact radius per inflow time:

$$Q \sim \frac{\pi GM_h \Sigma r_p}{t_{\text{infl}}} \sim \frac{\tau}{8\pi} \left(\frac{r_p}{r_g}\right)^{-1/2} \frac{t_{\text{orb}}}{t_{\text{infl}}} L_E, \quad (6)$$

where $L_E = 4\pi GM_h c / \kappa_T$ is the Eddington luminosity. The bottom-center panel of Figure 2 demonstrates that, apart from

an initial adjustment phase, this estimate is accurate to within a factor of ~ 2 .

In estimating t_{cool} , we ignore the contributions of radiation time and vertical advection for simplicity. In fact, finite radiation time slows cooling while vertical advection speeds it, hence the two effects partially cancel. The inner disk starts out optically thick, so

$$t_{\text{cool}} \sim \frac{\tau H}{c} \sim \frac{\tau}{4\pi} \left(\frac{r_p}{r_g}\right)^{-1/2} t_{\text{orb}}, \quad (7)$$

where we used $H/r_p \sim \frac{1}{2}$ in the second step. The inner disk eventually becomes so depleted that $\tau \lesssim 1$ and radiation can escape freely, at which point $L_c \sim Q$. This free-streaming limit is reached only when $t_{\text{infl}}/t_{\text{cool}} \gtrsim 1$, since $t_{\text{infl}} \gtrsim t_{\text{orb}}$ always and $t_{\text{cool}} \lesssim t_{\text{orb}}$ in this limit. Considering that L_c is capped by the minimum function in Equation (4) long before the free-streaming limit kicks in, the limit is irrelevant and we can use Equation (7) for all τ .

We see from Equation (7) that, as long as the inner disk maintains a high enough Σ to make

$$\tau \gtrsim 4\pi \left(\frac{r_p}{r_g}\right)^{1/2} \frac{t_{\text{infl}}}{t_{\text{orb}}}, \quad (8)$$

we have $t_{\text{infl}}/t_{\text{cool}} \lesssim 1$. Combining Equations (4), (6), and (7) in this regime yields

$$L_c/L_E \sim \frac{1}{2}. \quad (9)$$

This is our main result: The bolometric light curve of a TDE in an AGN starts off with an Eddington-level plateau. Our simulations confirm the validity of Equation (9): $Q t_{\text{inff}}/t_{\text{cool}}$ in the bottom-right panel of Figure 2 quickly stabilizes to $\sim L_E$. The remarkable constancy of L_c is due to the cancellation of t_{inff} and τ in the derivation of Equation (9) (see also Krolik 2010). When the inner disk is cleared out to the point that Equation (8) is violated and $t_{\text{inff}}/t_{\text{cool}} \gtrsim 1$, the luminosity falls as $L_c \sim Q \propto \Sigma$. Both the plateau duration and the post-plateau L_c depend on the time evolution of a single parameter, Σ .

Because the stream feeds the inner disk, the plateau duration is not limited by the initial inner disk mass and can be $\gg t_{\text{inff}}$; the plateau duration will be estimated in §4. A plateau may not appear if radiation time, convection, or magnetic buoyancy modifies the functional form of t_{cool} .

Our calculations give us only a crude estimate of the bolometric luminosity in some time-averaged sense. Accurate predictions of the light curve and the spectrum should be based on detailed radiation MHD simulations.

4. LIGHT CURVES

We consider two disk models for the unperturbed disk, depending on how the unperturbed accretion rate $\dot{M}_a \equiv L_a/(\eta c^2)$ compares with the Eddington accretion rate $\dot{M}_E \equiv L_E/(\eta c^2)$, where $\eta = 0.1$ is the fiducial radiative efficiency of a radiatively efficient disk. Any time-steady disk satisfies $\dot{M}_a \sim 4\pi r_p \Sigma_0 v_R$, where Σ_0 and v_R are the unperturbed surface density and radial velocity respectively. The value of Σ_0 is fixed by \dot{M}_d ; therefore, a choice of disk model boils down to a choice of v_R . The inflow mechanism in the unperturbed disk is the outward transport of angular momentum by internal stresses, but once the stream strikes the disk, inflow is driven by spiral shocks instead.

If $\dot{M}_a/\dot{M}_E \gtrsim 10^{-3}$, we assume the disk is geometrically thin, optically thick, and radiatively efficient (Shakura & Sunyaev 1973) with fiducial stress parameter $\alpha = 0.1$. Both the disk aspect ratio and v_R/v_ϕ at the impact point are $\ll 1$ in this model, v_ϕ being the orbital velocity. As a result, Σ_0 is large, and the initial energy dissipation rate Q_0 , obtained by substituting the unperturbed surface density Σ_0 into Equation (6), is large as well.

If \dot{M}_a/\dot{M}_E is any lower, the disk could be a geometrically thick, optically thin, radiatively inefficient accretion flow (RIAF) (e.g., Ichimaru 1977; Rees et al. 1982; Narayan & Yi 1994). Parameterizing the radial velocity in a geometrically thick disk as $v_R \sim \alpha' v_\phi$, we can write

$$\kappa_T \Sigma_0 \sim \frac{1}{\alpha' \eta'} \frac{L_a/L_E}{(r_p/r_g)^{1/2}}. \quad (10)$$

We emphasize that α' is merely a parameterization; for simplicity we take $\alpha' = 0.1$. Ryan et al. (2017) performed general relativistic MHD simulations of RIAFs assuming that electrons are heated by Coulomb scattering off ions at a rate derived empirically from solar wind measurements (Ressler et al. 2015). They found that the effective radiative efficiency is $\eta' \sim 10^{-2}$ for $\dot{M}_a/\dot{M}_E \sim 10^{-5}$, suggesting that accretion may proceed at efficiencies close to radiatively efficient values even at very low accretion rates. We adopt this value of η' below. The much larger v_R/v_ϕ in a RIAF compared to a radiatively efficient disk means that Σ_0 and hence Q_0 are much smaller.

The top panel of Figure 3 displays Q_0 for a radiatively efficient disk, and Figure 4 does the same for a RIAF. We end Figure 3 at $\dot{M}_a/\dot{M}_E = L_a/L_E = 10^{-4}$ and begin Figure 4 at $\dot{M}_a/\dot{M}_E = (\eta/\eta')(L_a/L_E) = 10^{-2}$ in view of the uncertain \dot{M}_a/\dot{M}_E marking the transition between the two disk models. The ridge of Q_0 follows from the fact that, in a radiatively efficient disk, Σ_0 reaches its maximum when disk pressure switches from gas- to radiation-dominated. Because $Q_0 \gtrsim L_E$ generally in a radiatively efficient disk, there is enough dissipation to power Eddington-level luminosity. By contrast, v_R is much larger and Σ_0 much smaller in a RIAF with the same \dot{M}_a/\dot{M}_E , so $Q_0 \ll L_E$. A noticeable flare is unlikely, so we drop the RIAF from further consideration.

The middle panel of Figure 3 plots the initial value of $t_{\text{inff}}/t_{\text{cool}}$ for the radiatively efficient disk, with t_{inff} and t_{cool} from Equations (5) and (7) respectively. For most of the parameter space plotted, $t_{\text{inff}}/t_{\text{cool}} \lesssim 1$, so $L_c \sim \frac{1}{2} L_E$ irrespective of M_h and L_a/L_E . With the gradual depletion of the inner disk, $t_{\text{inff}}/t_{\text{cool}} \propto 1/\Sigma$ rises but $Q \propto \Sigma/t_{\text{inff}}$ falls, and the two changes offset each other to sustain a constant L_c .

The luminosity plateau continues until $t_{\text{inff}}/t_{\text{cool}} \sim 1$. The plateau duration is calculated by applying Equation (8), the condition for a plateau. To connect τ in that equation to $\Sigma = \tau/\kappa_T$ in the simulations, we approximate $\Sigma(t)$ in the top-right panel of Figure 2 by

$$\Sigma/\Sigma_0 \sim 0.1 (t/t_{\text{dec}})^\gamma \quad \text{for } t \gtrsim t_{\text{dec}}, \quad (11)$$

with $t_{\text{dec}} = 10$ d the start of the approximately power-law decay and $\gamma = -2.5$ the power-law index. If $t_{\text{inff}}/t_{\text{cool}} \gtrsim 0.1$ initially, this equation allows us to determine only an upper limit of $\lesssim 10$ d to the plateau duration. The plateau duration is shown in the bottom panel of Figure 3, and explicit expressions can be found in Appendix A. The plateau typically lasts tens of days. After the plateau, the inner disk fades as $L_c \sim Q \propto \Sigma$. For a small part of the parameter space, $t_{\text{inff}}/t_{\text{cool}} \gtrsim 1$ even at the beginning; these inner disks do not have a luminosity plateau.

The plateau duration is comparable to but typically smaller than t_{mb} . Although the stream mass current decreases during the plateau, the disk mass current would decrease by an even greater amount, according to Equation (11). Therefore, the stream would become heavier and heavier relative to the disk as the event progresses, so the assumption that energy dissipation in the disk dominates that in the stream remains valid.

For a radiatively efficient unperturbed disk, Figure 3 shows that the maximum plateau duration of ~ 23 d is found at $M_h \sim 4 \times 10^6 M_\odot$ and $L_a/L_E \sim 10^{-3}$. The disk giving rise to the longest plateau is marginally radiatively efficient, and its pressure at the stream impact radius is on the cusp between gas and radiation dominance; such a disk has the greatest Σ_0 and thus the longest t_{cool} . The numbers here are for the fiducial case of a Sun-like star, but the argument holds for other main-sequence stars as well. As detailed in Appendix A and illustrated in Figure 6, the maximum plateau duration and the corresponding M_h increase with M_\star as $(M_\star/M_\odot)^{1-1/(12\gamma)}$ and $(M_\star/M_\odot)^{7/8}$ respectively.

Figure 5 displays the estimated bolometric light curves for four radiatively efficient unperturbed disks. For all four, the luminosity plateau lasts ~ 20 d to within a factor of ~ 1.5 . After the plateau, $L_c \sim Q \propto \Sigma \propto t^\gamma$. The power-law index of the falloff is steeper than $-\frac{5}{3}$, the power-law index of the mass return

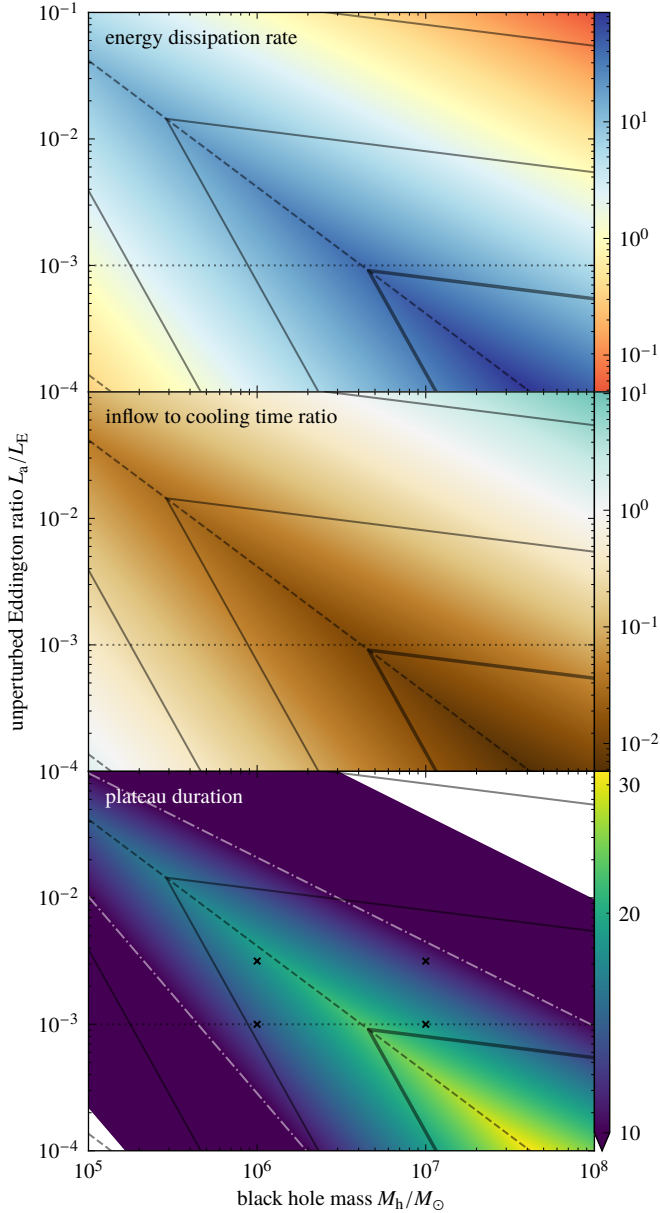


Figure 3. Color contours of three properties of the perturbed inner disk, as functions of the black hole mass M_h and the Eddington ratio L_a/L_E of the unperturbed disk, with other parameters fixed at their fiducial values (§§2 and 4). This figure portrays the case in which the unperturbed inner disk is a radiatively efficient disk, while Figure 4 illustrates the case of a RIAF. The top panel shows the initial energy dissipation rate Q_0 divided by the Eddington luminosity L_E . The middle panel shows the initial value of the ratio of inflow to cooling time $t_{\text{infl}}/t_{\text{cool}}$. The bottom panel shows the plateau duration in units of days (Appendix A). The blue regions outside the dash-dotted lines have only an upper limit, while the empty regions have no plateau at all because $t_{\text{infl}}/t_{\text{cool}} \gtrsim 1$ initially. The crosses are the values of $(M_h, L_a/L_E)$ for which light curves are shown in Figure 5. In all panels, the lower dashed line at $L_a \sim 1.7 \times 10^{39} \text{ erg s}^{-1}$ separates two opacity regimes of the unperturbed disk: opacity is dominated by free-free absorption below and electron scattering above. The upper dashed line at $L_a \sim 5 \times 10^{41} \text{ erg s}^{-1}$ separates two pressure regimes of the unperturbed disk: pressure is dominated by gas below and radiation above. The thick gray chevron is the contour for $\dot{M}_s/\dot{M}_d = 1$, and the two thin ones above it are for $\dot{M}_s/\dot{M}_d = 10$ and $\dot{M}_s/\dot{M}_d = 100$ respectively. Our approximation that the stream has greater inertia than the disk holds for \dot{M}_s/\dot{M}_d above a few tenths (Chan et al. 2019). The horizontal dotted line marks the value of L_a/L_E below which the radiatively efficient disk may become a RIAF.

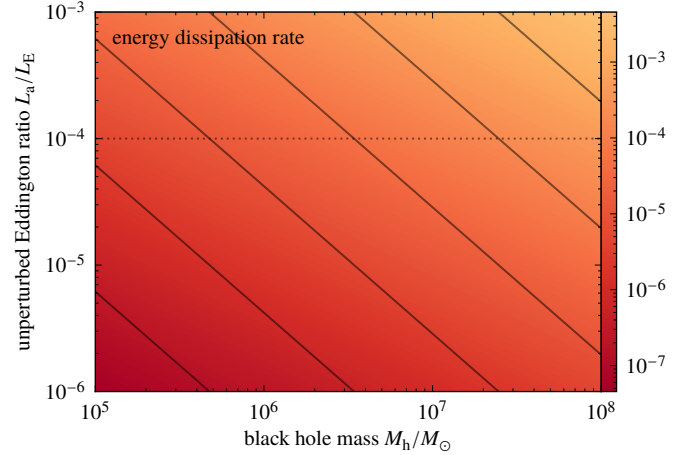


Figure 4. Color contours of the initial energy dissipation rate Q_0 divided by the Eddington luminosity L_E , as functions of the black hole mass M_h and the Eddington ratio L_a/L_E of the unperturbed disk, with other parameters fixed at their fiducial values (§§2 and 4). This figure portrays the case in which the unperturbed inner disk is a RIAF, while Figure 3 illustrates the case of a radiatively efficient disk. Gray contours are drawn at constant levels of unperturbed \dot{M}_s/\dot{M}_d , starting from 10^4 in the top-right and increasing by a factor of 10 for each contour toward the bottom-left. The horizontal dotted line marks the value of L_a/L_E above which the RIAF may become a radiatively efficient disk.

rate (Phinney 1989), and the two are completely unrelated.

5. DISCUSSION

The Eddington-level luminosity plateau discussed here is qualitatively different from the plateaus in other TDE models. The classical picture (e.g., Rees 1988) describes a TDE around an isolated black hole. The debris, returning to pericenter at super-Eddington rates for up to several years (e.g., Evans & Kochanek 1989), quickly forms a circular disk. The disk bolometric luminosity tracks the mass return rate, but instead of going super-Eddington, it reaches a plateau (e.g., Loeb & Ulmer 1997; Krolik & Piran 2012). It should be noted that the classical picture has been called into question by simulations (Shiokawa et al. 2015) and their implications for observations (Piran et al. 2015; Krolik et al. 2020). In particular, the predicted plateau is not seen in the light curves of most optical TDEs (van Velzen et al. 2020), and its existence is under debate.

The stream-disk interaction we discussed applies to a TDE around a black hole with a pre-existing accretion disk. In contrast with the classical picture, the plateau is produced when the debris slams into the disk, and the principal parameter determining whether and for how long our plateau can be observed is the accretion rate of the unperturbed disk. Moreover, the plateau is shorter than in the classical picture, lasting only tens of days. One respect in which our mechanism does resemble the classical picture, however, is that the plateaus in both cases arise from radiation trapping, that is, a situation in which inflow is faster than radiation can escape by diffusion.

Saxton et al. (2019) reported a TDE candidate in a quiescent galaxy with a $\sim 10^7 M_\odot$ black hole. The 0.2-to-2 keV flux held steady for ~ 90 d at a $\sim 10^{-3}$ Eddington level before diminishing as a power law. If the galaxy were to harbor a weakly accreting black hole with no recognizable AGN signatures, then

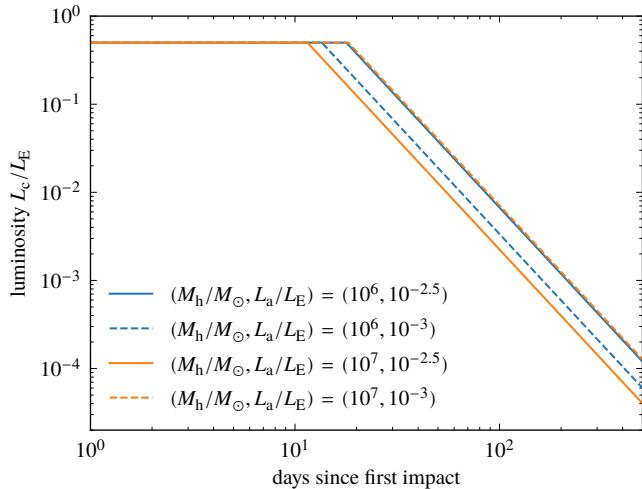


Figure 5. Estimated bolometric light curves assuming that the unperturbed disk is radiatively efficient. The level of the initial plateau is given by Equation (9), and the plateau duration by the bottom panel of Figure 3. That panel also shows, with crosses, $(M_h/M_\odot, L_a/L_E)$ of the depicted light curves. The plateau duration depends weakly on M_h and L_a/L_E , and the dependence changes sign when disk pressure transitions from gas- to radiation-dominated (Appendix A). The longest plateau duration for radiatively efficient disks across all M_h and L_a/L_E is ~ 23 d (Figure 3); the light curves here come close to that limit.

the disruption of a $\sim 4 M_\odot$ main-sequence star could produce a plateau with the observed duration. The dimness of the plateau may be explained by most of the energy being radiated at other frequencies, or by dust extinction.

Our simulations did not account for magnetic fields. Magnetic field loops in the outer disk can protrude into the depleted inner disk (Noble et al. 2011), enhancing magnetic stresses to the degree that the outer disk may replenish the inner disk on a timescale as fast as a few days. Any resupply from the outer disk complements resupply from the stream, keeping Σ at a high level and prolonging the plateau.

Our calculations do not capture the gradual increase of the stream mass current to its peak value in realistic TDEs. During the early parts of this rising phase when the stream is lighter than the disk, our predictions here do not apply, but shocks excited by the light stream can still deflect orbiting disk material toward the black hole. Therefore, at later times when the stream is heavier than the disk and our predictions do apply, the disk will have a surface density smaller than its unperturbed value, suggesting that any luminosity plateau that may appear would be shorter. However, if the net mass loss from the inner disk during the rising phase is small due to resupply from the stream or the outer disk, the plateau might be extended. Exactly how a time-varying stream mass current affects the light curve is the subject of future simulations.

Even though predictions about the spectrum of the inner disk are of great astrophysical interest, we refrain from making such predictions because the spectrum depends sensitively on the structure of the inner disk and its cooling mechanisms, but we have little knowledge of either. The comparable magnitudes of t_{inff} and t_{cool} mean that gas and radiation energy densities in the inner disk vary on similar timescales, and the vigorous energy dissipation in the inner disk implies that radiation pressure may be instrumental in shaping the inner disk. A careful treatment

of the inner disk therefore requires computationally expensive radiative MHD simulations that can evolve gas and radiation in unison. Radiative transfer must be performed in three dimensions on account of the lack of symmetry: shocks are localized and heating is uneven; the disk structure shown in Figure 1 is highly irregular, both along the midplane and in the vertical direction; and the stream arches over and partly occludes the disk. It is also unclear to what degree free-free and Compton processes bring the disk to thermal equilibrium. In light of all these considerations, we content ourselves with an estimate of the light curve, which already has a very distinctive shape.

6. CONCLUSIONS

The black hole of an AGN is surrounded by an accretion disk. The debris stream of a TDE around such a black hole runs into the disk near pericenter. The stream delivers a much stronger mass current to the impact point than the disk does, so the dynamical evolution of the former is largely unaffected by the latter. On the other hand, the heavy stream prevents the disk from rotating freely. Shocks are formed where the disk smashes into the stream; disk gas is deflected inward and drives shocks against gas closer in. As a result, the kinetic energy of the disk interior to the impact point is dissipated into internal energy at a rate high enough to power a bright flare.

If the unperturbed disk is radiatively efficient, that is, if its luminosity is $\gtrsim 10^{-3}$ Eddington, then the disk surface density Σ is large enough to make the initial energy dissipation rate $Q \propto \Sigma$ super-Eddington. Conversely, if the unperturbed disk is a RIAF, Σ is too small and Q too low to beget any visible flare.

Because gas in the inner disk falls into the black hole in only a few orbits, not all the energy dissipated issues forth as radiation. We estimate the bolometric luminosity as $L_c \sim Q \min(1, t_{\text{inff}}/t_{\text{cool}})$, where t_{inff} is the time for a gas packet to flow inward from the impact point to the black hole, and t_{cool} is the cooling time of the inner disk. The luminosity at early times is regulated to an Eddington-level plateau by the facts that $Q \propto \Sigma/t_{\text{inff}}$ and $t_{\text{cool}} \propto \Sigma$.

The luminosity plateau ends when $t_{\text{inff}}/t_{\text{cool}}$ falls to ~ 1 , which occurs after the disk has been depleted by shock-driven inflows. Resupply from the stream and the outer disk could keep both Σ and t_{cool} large, delaying the end of the plateau. If only stream resupply acts, as in our simulations, then the plateau duration is largely determined by the initial Σ , which is greatest for marginally radiatively efficient disks in which gas and radiation contribute comparably to the pressure. The maximum plateau duration is $\sim 23 \text{ d} \times (M_\star/M_\odot)$, produced by a TDE around a $\sim 4 \times 10^6 M_\odot \times (M_\star/M_\odot)^{7/8}$ black hole.

Following the end of the plateau, $L_c \propto \Sigma$, which in our simulations declines as a power law in time with index between -3 and -2 at earlier times, and possibly a steeper index at later times.

Lastly, the simulations of Chan et al. (2019) show that part of the stream drills through the disk and fans out on the other side into a dilute plume, a fraction of which crashes back and collides inelastically with the disk. The resulting luminosity enhancement, which could also be a fraction of Eddington at early times, will be characterized in future work.

The authors thank Kojiro Kawana for the question that prompted

this investigation, and Tatsuya Matsumoto and Alexander Dittmann for fruitful discussions. This work was partially supported by ERC advanced grant ‘‘TRex’’ (CHC and TP) and NSF grant AST-1715032 (JHK).

APPENDIX

A. PLATEAU DURATION

We present explicit expressions, applicable to all stars, for the plateau duration when the unperturbed disk is radiatively efficient (Shakura & Sunyaev 1973). Because r_t depends on M_\star and r_\star , we generalize t_{dec} in Equation (11) to

$$t_{\text{dec}} = 10 \text{ d} \times \left(\frac{M_\star}{M_\odot} \right)^{-1/2} \left(\frac{r_\star r_p}{r_\odot r_t} \right)^{3/2}. \quad (\text{A1})$$

If the unperturbed disk is dominated by gas pressure and Thomson scattering opacity at the stream impact radius, the plateau duration is

$$\sim 14 \text{ d} \times \left(\frac{M_\star}{M_\odot} \right)^{-1/2-11/(30\gamma)} \left(\frac{r_\star r_p}{r_\odot r_t} \right)^{3/2+11/(10\gamma)} \times \left[\left(\frac{M_h}{10^6 M_\odot} \right)^{-14/15} \left(\frac{L_a/L_E}{10^{-3}} \right)^{-3/5} \left(\frac{\alpha}{0.1} \right)^{4/5} \left(\frac{\eta}{0.1} \right)^{3/5} \right]^{1/\gamma}, \quad (\text{A2})$$

where $\gamma = -2.5$ from Equation (11). If the unperturbed disk is dominated instead by radiation pressure and Thomson scattering opacity, the plateau duration is

$$\sim 18 \text{ d} \times \left(\frac{M_\star}{M_\odot} \right)^{-1/2+1/(3\gamma)} \left(\frac{r_\star r_p}{r_\odot r_t} \right)^{3/2-1/\gamma} \times \left[\left(\frac{M_h}{10^7 M_\odot} \right)^{2/3} \left(\frac{L_a/L_E}{10^{-3}} \right) \left(\frac{\alpha}{0.1} \right) \left(\frac{\eta}{0.1} \right)^{-1} \right]^{1/\gamma}. \quad (\text{A3})$$

Because Equation (11) is valid only for $t \gtrsim t_{\text{dec}}$, a plateau duration shorter than that should be interpreted as an upper limit at t_{dec} .

Equations (A2) and (A3) are plotted in the bottom panel of Figure 3 for the fiducial case of a Sun-like star, and in Figure 6 for other main-sequence stars obeying $r_\star \propto M_\star$. The maximum plateau duration is

$$\sim 23 \text{ d} \times \left(\frac{M_\star}{M_\odot} \right)^{-1/2+1/(24\gamma)} \left(\frac{r_\star r_p}{r_\odot r_t} \right)^{3/2-1/(8\gamma)}, \quad (\text{A4})$$

which is attained at

$$M_h \sim 4 \times 10^6 M_\odot \times \left(\frac{M_\star}{M_\odot} \right)^{-7/16} \left(\frac{r_\star r_p}{r_\odot r_t} \right)^{21/16}. \quad (\text{A5})$$

REFERENCES

Chan, C.-H., Piran, T., Krolik, J. H., & Saban, D. 2019, *ApJ*, **881**, 113
 Evans, C. R., & Kochanek, C. S. 1989, *ApJL*, **346**, L13
 Hills, J. G. 1975, *Natur*, **254**, 295
 Ichimaru, S. 1977, *ApJ*, **214**, 840
 Kathirgamaraju, A., Barniol Duran, R., & Giannios, D. 2017, *MNRAS*, **469**, 314
 Kochanek, C. S. 1994, *ApJ*, **422**, 508

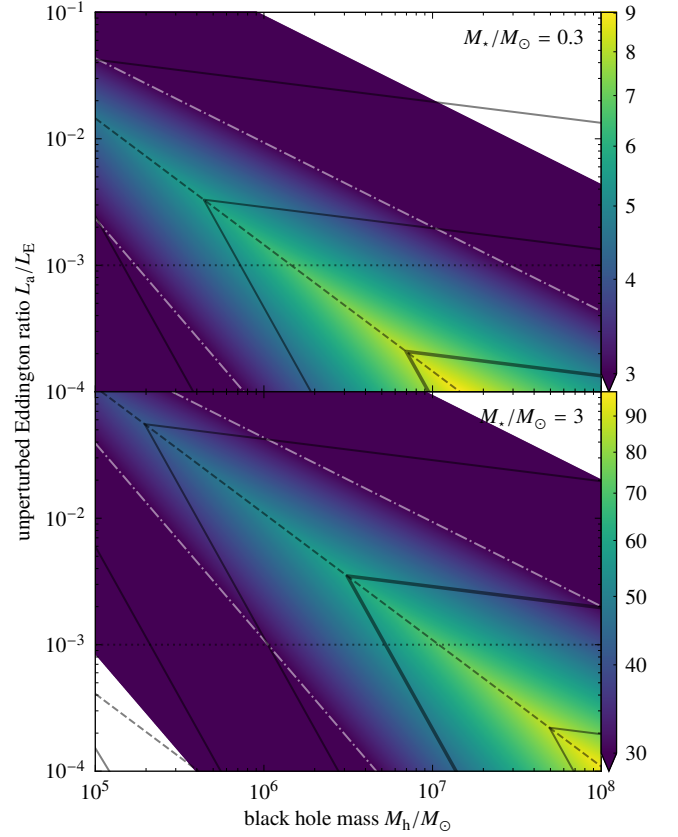


Figure 6. Same as the bottom panel of Figure 3, but for different main-sequence stars with masses as indicated in the top-right corner of each panel. The plateau is longer for more massive stars. The gray chevrons are contours of constant \dot{M}_s/\dot{M}_d ; they increase by factors of 10 toward the top left, and the thick one is for $\dot{M}_s/\dot{M}_d = 1$. The contours slide upward with rising M_\star . Our approximation that the stream has greater inertia than the disk holds for \dot{M}_s/\dot{M}_d above a few tenths (Chan et al. 2019).

Krolik, J., Piran, T., & Ryu, T. 2020, arXiv: 2001.03234
 Krolik, J. H. 2010, *ApJ*, **709**, 774
 Krolik, J. H., & Piran, T. 2012, *ApJ*, **749**, 92
 Loeb, A., & Ulmer, A. 1997, *ApJ*, **489**, 573
 Narayan, R., & Yi, I. 1994, *ApJL*, **428**, L13
 Noble, S. C., Krolik, J. H., Schnittman, J. D., & Hawley, J. F. 2011, *ApJ*, **743**, 115
 Phinney, E. S. 1989, in Symposium of the International Astronomical Union, Vol. 136, *The Center of the Galaxy*, ed. M. Morris (Netherlands: Springer), 543–553
 Piran, T., Svirski, G., Krolik, J., Cheng, R. M., & Shiokawa, H. 2015, *ApJ*, **806**, 164
 Rees, M. J. 1988, *Natur*, **333**, 523
 Rees, M. J., Begelman, M. C., Blandford, R. D., & Phinney, E. S. 1982, *Natur*, **295**, 17
 Ressler, S. M., Tchekhovskoy, A., Quataert, E., Chandra, M., & Gammie, C. F. 2015, *MNRAS*, **454**, 1848
 Ryan, B. R., Ressler, S. M., Dolence, J. C., et al. 2017, *ApJL*, **844**, L24
 Ryu, T., Krolik, J., Piran, T., & Noble, S. C. 2020, arXiv: 2001.03501
 Saxton, R. D., Read, A. M., Komossa, S., et al. 2019, *A&A*, **630**, A98
 Shakura, N. I., & Sunyaev, R. A. 1973, *A&A*, **24**, 337
 Shiokawa, H., Krolik, J. H., Cheng, R. M., Piran, T., & Noble, S. C. 2015, *ApJ*, **804**, 85

Van Velzen, S., Gezari, S., Hammerstein, E., et al. 2020, arXiv:
[2001.01409](https://arxiv.org/abs/2001.01409)